Acta Pharmaceutica Sinica B 2023;13(1):425−439

Chinese Pharmaceutical Association
Institute of Materia Medica, Chinese Academy of Medical Sciences

Acta Pharmaceutica Sinica B

www.elsevier.com/locate/apsb
www.sciencedirect.com

ORIGINAL ARTICLE

Sialic acid-mediated photochemotherapy enhances infiltration of CD8$^+$ T cells from tumor-draining lymph nodes into tumors of immunosenescent mice

Dezhi Sui, Changzhi Li, Xueying Tang, Xianmin Meng, Junqiang Ding, Qiongfen Yang, Zhaowei Qi, Xinrong Liu, Yihui Deng, Yanzhi Song*

College of Pharmacy, Shenyang Pharmaceutical University, Shenyang 110016, China

Received 2 March 2022; received in revised form 23 April 2022; accepted 18 May 2022

KEY WORDS

Immunosenescence;
Sialic acid;
Photochemotherapy;
CD8$^+$ T cells;
Doxorubicin;
Neutrophils;
Indocyanine green;
Liposomes

Abstract Immunoscenescence plays a key role in the initiation and development of tumors. Furthermore, immunoscenescence also impacts drug delivery and cancer therapeutic efficacy. To reduce the impact of immunosenescence on anti-tumor therapy, this experimental plan aimed to use neutrophils with tumor tropism properties to deliver sialic acid (SA)-modified liposomes into the tumor, kill tumor cells *via* SA-mediated photochemotherapy, enhance infiltration of neutrophils into the tumor, induce immunogenic death of tumor cells with chemotherapy, enhance infiltration of CD8$^+$ T cells into the tumor-draining lymph nodes and tumors of immunosenescent mice, and achieve SA-mediated photochemotherapy. We found that CD8$^+$ T cell and neutrophil levels in 16-month-old mice were significantly lower than those in 2- and 8-month-old mice; 16-month-old mice exhibited immunosenescence. The anti-tumor efficacy of SA-mediated non-photochemotherapy declined in 16-month-old mice, and tumors recurred after scabbing. SA-mediated photochemotherapy enhanced tumor infiltration by CD8$^+$ T cells and neutrophils, induced crusting and regression of tumors in 8-month-old mice, inhibited metastasis and recurrence of tumors and eliminated the immunosenescence-induced decline in antitumor therapeutic efficacy in 16-month-old mice *via* the light-heat-chemical-immunity conversion.

*Corresponding author.
E-mail address: songyanzhi@syphu.edu.cn (Yanzhi Song).

Peer review under responsibility of Chinese Pharmaceutical Association and Institute of Materia Medica, Chinese Academy of Medical Sciences.

https://doi.org/10.1016/j.apsb.2022.06.005

1. Introduction

The world population is aging, and the problems associated with old age are becoming increasingly serious[1]. After the COVID-19 outbreak, the high disease susceptibility and lower ability to recover of the elderly have resulted in high infection and mortality rates[2−4]. The problems associated with treating disease in the elderly have become increasingly prominent, and Nature Publishing Group has established a new sub-journal called *Nature Aging* to promote the dissemination of research findings in this area[5]. Aging results in the immune system gradually undergoing a series of degenerative changes stemming from the long-term combined action of multiple factors; this is called immunosenescence[6]. T lymphocyte aging is the main manifestation of immunosenescence[7]. A host of clinical data show that the health of the human body is closely related to T lymphocyte function and that T lymphocyte aging is the main cause of disease in the elderly[8]. T lymphocyte functioning is age-dependent, and their ability to recognize and eliminate harmful entities (such as microorganisms or malignant cells) is significantly reduced with age[9]. $CD8^+$ T cells aging caused by immunosenescence in tumor-draining lymph nodes (TDLNs) makes it more likely that tumor cells will be able to evade immune recognition and elimination, thereby allowing them to continue to proliferate and increasing the possibility of cancer recurrence after treatment[10]. Additionally, innate immune cells (*e.g.*, neutrophils, monocytes, and NK cells) are also affected by immunosenescence (see Scheme 1).

Most immunosenescence studies to date have focused on the aging of the immune system and the underlying mechanisms[11]. The impacts of immunosenescence on the therapeutic efficacy of some age-related diseases (especially cancer) have, however, remained largely unexplored. In preclinical antitumor therapy studies, mice that are aged 4−8 weeks (equivalent to humans aged 1−16 years) are used as laboratory animals; however, this age does not match that of clinical patients. Clinical data indicate that the peak incidence of cancer in humans is at 50−70 years of age[12]. Immunosenescence greatly affects the distribution of nano-drugs that are closely related to the immune system. The development and application of cancer nano-drugs have, therefore, been stymied by the lack of immunosenescence research to date[13−15]. In the past 20 years, our research group has been investigating the close relationship between the immune system and nano-drugs, and we have systematically researched SA-modified nanoparticles (NPs), which can be administered by neutrophils-mediated drug delivery[16−18]. Photodynamic/Photothermal therapy (PDT/PTT) increased the accumulation of SA-modified NPs in the tumor by enhancing tumor infiltration by neutrophils[19]. SA-modified DOX liposomes prepared in our laboratory-induced the expression of calreticulin (CRT), increased the secretion of HMGB-1, and promoted the release of ATP from tumor cells[20]. Dendritic cells recognize and phagocytize tumor cells, enhance the ability of $CD8^+$ T cells to infiltrate tumors, and attack the tumor cells[21]. Immunogenic cell death (ICD) of tumor cells can transform immunosuppressive or 'cold' tumors into immune-infiltrating 'hot' tumors, and some mice can even achieve tumor regression[20]. However, the above research results were all obtained in mice aged 4−8 weeks, without considering the potential impact of immunosenescence on therapeutic efficacy.

SA-modified liposomes achieve antitumor effects by interacting with immune cells (T cells, neutrophils, and monocytes)[20,22,23]. Using these liposomes as carriers to deliver drugs can help elucidate the immunosenescence-induced change in the antitumor therapeutic efficacy of phototherapy or chemotherapy. We prepared SA-modified doxorubicin (DOX)-loaded liposomes, SA-modified indocyanine green (ICG)-loaded liposomes, and SA-modified DOX and ICG co-loaded liposomes to treat C57BL/6JNifdc mice with melanoma (B16/F10 cells) that were either 2 months (adolescent, human equivalent of 16 years), 8 months (adult, human equivalent of 33 years), or 16 months (old, human equivalent of 60 years) old[24].

We found that 16-month-old mice exhibited immunosenescence, which affected the antitumor therapeutic efficacy of phototherapy and chemotherapy. However, SA-mediated photochemotherapy eliminated the decline in the antitumor therapeutic efficacy of phototherapy or chemotherapy caused by immunosenescence.

2. Materials and methods

2.1. Reagents, animals and cells

B16/F10 and HL-60 cells were purchased from the Cell Bank of the Chinese Academy of Sciences (Shanghai, China). B16/F10 and HL-60 cells were cultured in RPMI 1640 medium (Procell Life Science&Technology Co., Ltd., WH0221k031, Wuhan, China) containing 10% FBS (Gemini Bio, A24G00J, Calabasas, CA, USA). Female C57BL/6JNifdc mice aged 2, 8, and 16 months were purchased from Beijing Weitonglihua Laboratory Animal Technology Co., Ltd. (No.110011211103615527, No.110011211100204365, Beijing, China). All experimental procedures were executed according to the protocols approved by Shenyang Pharmaceutical University Animal Care and Use Committee.

2.2. Preparation of SA-modified liposomes

SA-modified liposomes were prepared by thin-film evaporation[25]. Hydrogenated soybean phosphotidylcholine (HSPC, AVT (Shanghai) Pharmaceutical Tech Co., Ltd., C10695, Shanghai, China), dipalmitoyl phosphatidylcholine [DPPC, AVT (Shanghai) Pharmaceutical Tech Co., Ltd., B91150, Shanghai, China], cholesterol (CH, Xinbai Pharmaceutical Co., Ltd., 120502, Nanjing, China), indocyanine green (ICG, Dalian Meilun Biological Co., Ltd., A0807A, Dalian, China), and MT-18 were dissolved in 10% final volume (*v*/*v*) of liposomes in anhydrous methanol. A rotary evaporator (Zhengzhou Keda Machinery Instrument Equipment Co., Ltd., RE-501, Zhengzhou, China) was used to remove the organic solvents in a 60 °C water bath for 5 min. A desktop vacuum drying oven (Shanghai Jiecheng Experimental Instrument Co., Ltd., DZF-6020, Shanghai, China) was used to remove the residual methanol at 60 °C for 8 h. An ammonium sulfate solution (200 mmol/L) containing 5% methanol was added, and the mixture was stirred at 60 °C for 20 min. An ultrasonic cell pulverizer (200 W for 2 min, 400 W for 8 min; Ningbo Xinzhi Biotechnology Co., Ltd., Scientz-950E, Ningbo, China) was used to obtain the initial liposome preparations. Initial liposomes samples (100 μL) were added to the top of an anion-cation mixed-fiber column to remove free drug (1: 1, *v*/*v*, Guilin Zhenghan Science and Technology Development Co., Ltd., Guilin, China); the mixture was allowed to stand for 2 min, and a centrifuge (Xiangyi Centrifuge Instrument Co., Ltd., L 530, Changsha,

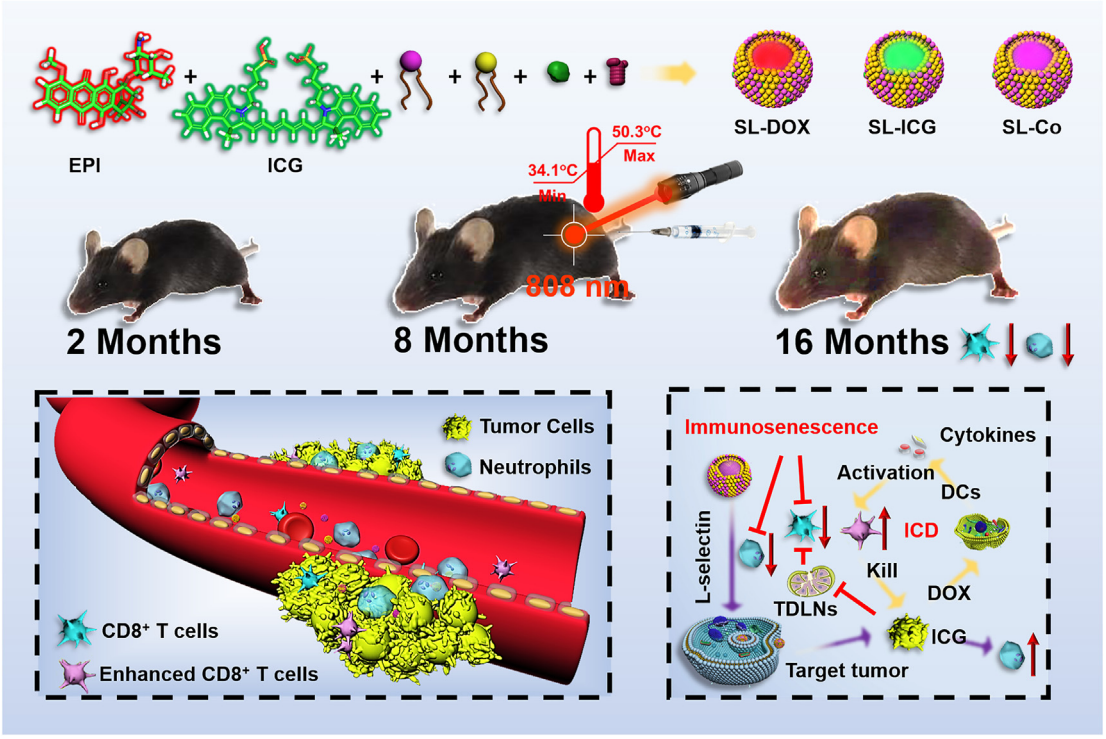

Scheme 1 Schematic illustration of the construction, neutrophils-mediated drug delivery system, and immunosenescence-mediated antitumor therapeutic efficacy of SL-DOX/SL-ICG/SL-Co. Therapeutic effect of SL-Co could simultaneously enhance the infiltration of $CD8^+$ T cells and neutrophils into the tumor, increased the accumulation of drugs at the tumor site, improved the effect of antitumor therapy, and eliminated the decline in anti-tumor therapeutic efficacy in 16-month-old mice caused by immunosenescence.

China) was used to centrifuge the mixture at 500×*g* for 4 min. Then, 50 μL of sterile water was added for injection, centrifuged at 500×*g* for 4 min, and elution was repeated twice with water. After being passed through 0.80-, 0.45-, and 0.22-μm microporous membranes, the resulting product was mixed with 1 mL of DOX (Beijing HVSF United Chemical Material Co., Ltd., HF190916, Beijing, China) solution (10 mg/mL) and incubated in a 60 °C water bath for 20 min. The above process was repeated, and an anion-cation mixed-fiber column was used to remove the free drug. SA-modified ICG and DOX co-loaded liposomes (SL-Co) were obtained. Before use, 1 mL of the prepared liposomes was placed in a dialysis bag (Shanghai Yuanye Biotechnology Co., Ltd., 10 kDa, Shanghai, China) and dialyzed against 500 mL of 5% sucrose solution for 4 h, with a change of the dialysate every 2 h. SL-Co was mixed with 10 mg/mL DiR (Dalian Meilun Biological Co., Ltd., D122OA, Dalian, China) absolute ethanol solution and then stirred at 60 °C for 20 min to prepare SA-modified triple-loaded liposomes (0.2 mg/mL DiR, SL-DiR).

The hydration medium was replaced with a 200 mmol/L ammonium sulfate solution and the above steps were repeated to prepare SA-modified DOX-loaded liposomes (SL-DOX). Similarly, the hydration medium was replaced with a 5% methanol solution and the above steps were repeated to prepare SA-modified ICG-loaded liposomes (SL-ICG).

2.3. *Characterization of SA-modified liposomes*

A Nicomp-380 dynamic light scattering particle sizer (PSS, Nicomp-380, Pleasanton, CA USA) was used to measure the particle size and *Zeta* potential of the diluent after SL-DOX, SL-ICG, and SL-Co were diluted 200 times with sterile water for injection.

Transmission electron microscopy (TEM) images of the liposomes were acquired using the microscope (JEOL Corporation, JEM-2100, Tokyo, Japan). Then, 10 μL of liposomes were placed on a 200-mesh copper grid and allowed to stand for 5 min. Subsequently, 2% phosphotungstic acid solution was added and allowed to react for 3 min for staining.

The photothermal effect of liposomes was recorded using a thermal imaging camera (FLIR Systems, Inc., FLIR TG167, Portland, OR, USA). Then, 200 μL aliquots of SL-DOX, SL-ICG, or SL-Co were added to a 0.5 mL EP tube and irradiated (2 W/cm^2) with an 808 nm laser (Changchun New Industries, MDL-H-808-4W, Changchun, China) for 3 min, and the temperature variation of the solution in the EP tube was observed.

An ultraviolet−visible spectrophotometer (Beijing Ruili Analytical Instrument Co., Ltd., UV1801, Beijing, China) was used to determine the encapsulation efficiency. Then, 200 μL aliquots of SL-DOX, SL-ICG, or SL-Co without free drug were added separately to 10 mL volumetric flasks. Next, 100 μL of liposomes with free drug and 100 μL of sterile water for injection were added separately to 10 mL volumetric flasks. After constant volume demulsification of methanol, the absorbance (A_0) of liposomes with free drug and the absorbance (A_1) of liposomes without free drug (DOX: 480 nm, ICG: 784 nm) were measured and the encapsulation rate (EE) was calculated using Eq. (1):

$$\mathrm{EE}\ (\%) = A_0/A_1 \times 100 \quad (1)$$

The ultraviolet−visible spectrophotometer (Beijing Ruili Analytical Instrument Co., Ltd.) was used to determine the cumulative release rate. Then, 2.0 mL aliquots of SL-DOX, SL-ICG, SL-Co, or SL-DOX after 808 nm laser irradiation for 3 min (La-DOX, 2 W/cm^2; La-ICG, 2 W/cm^2; La-Co, 2 W/cm^2) were added separately to 10 kDa dialysis bags, which were placed in a dissolution cup containing 198 mL 5% sucrose solution. The mixture was stirred at a constant speed of 75 rpm at 37 ± 1 °C, and 4 mL of the dialysate was removed at 0, 1, 3, 6, 9, 12, 24, and 48 h. The same amount of the release medium was added at 37 ± 1 °C. The ultraviolet−visible spectrophotometer was used to determine the DOX concentration and cumulative release rate (n = 3). We repeated the above release experiment. Then, 100 μL of liposomes from the dialysis bag was removed, and the amount of ICG released from the liposomes was determined by measurement of the encapsulation efficiency of ICG.

2.4. Cytotoxicity and wound-healing assay

CCK-8 reagent (Dalian Meilun Biological Co., Ltd., MAO218-2-Jul-07G, Dalian, China) was used to determine the cytotoxicity toward B16/F10 cells. B16/F10 cells in logarithmic growth phase were added to a serum-free medium to prepare cell suspensions (1 × 10^6 cells/mL). In addition to the blank and preparation wells, 100 μL of cell suspension (1 × 10^6 cells/mL) was added to a 96-well plate and incubated for 12 h at 37 °C in a 5% CO_2 cell incubator. Serum-free medium containing various concentrations of liposomes was added and incubated for 48 h. CCK-8 reagent was added and the absorbance was measured 3 h later at 450 nm using a microplate reader (Bio-Rad, Model 680, Hercules, CA, USA). We calculated the Cell viability (%), IC_{50} values, and combination index (CI), as shown in Eqs. (2) and (3).

$$\text{Cell viability}\ (\%) = (OD_{sample} - OD_{preparation})/(OD_{control} - OD_{blank}) \times 100 \quad (2)$$

$$CI = [CA]_{50}/[A]_{50} + [CB]_{50}/[B]_{50} \quad (3)$$

A cell-free area was generated in the B16/F10 cells monolayer to determine their migration rate. Briefly, 1 mL of cell suspension (1 × 10^6 cells/mL) was added to a 6-well plate. After being cultured in a 37 °C, 5% CO_2 cell incubator for 12 h, a 10 μL pipette tip was used to generate cell-free areas in the monolayer, and serum-free medium containing liposomes (DOX final concentration: 50 μg/mL, ICG final concentration: 20 μg/mL), which has been subjected to 808 nm laser irradiation for 3 min (2 W/cm^2), was added. The width of the cell-free areas was determined using an inverted microscope at 0, 6, 12, and 24 h.

2.5. Isolation of T lymphocytes and neutrophils

2.5.1. Isolation of T lymphocytes

The grind-sieve method was used to isolate $CD8^+$ T cells from the TDLNs (from the lateral fold to the thigh muscle tissue, close to the deep iliac circumflex branch, n = 3) of mice of different ages[26]. The TDLNs were dissected and placed in a centrifuge tube containing 1 mL PBS. The thymus tissue was disintegrated by repeated scraping over a metal grid, tissue debris was removed through a mesh cell screen (5 cm × 5 cm); the filtrate was mixed with an equal volume of red blood cell lysate and paced at 4 °C for 5 min. It was then centrifuged at 1000×g for 4 min to collect the cells, and subsequently, 200 μL of PBS containing 1 μL PE-conjugated anti-mouse CD8 antibody (Bio-Legend, B266455, San Diego, CA, USA) and 1 μL FITC-conjugated anti-mouse CD3 antibody (Bio-Legend, B274724, San Diego, CA, USA) were added and the sample incubated for 30 min. The total number of isolated cells in the TDLNs was counted using a hemocytometer, and the variation in $CD8^+$ T cells in the isolated cell samples was determined by flow cytometry.

The grind-sieve method was used to isolate T lymphocytes from the thymus of 2-, 8-, and 16-month-old mice (n = 3). Using the above isolation method for T lymphocytes, $CD3^+$ T cells in the thymus were labeled and measured.

2.5.2. Isolation of neutrophils

Density gradient centrifugation was used to isolate neutrophils from the tibia and femur of 2-, 8-, and 16-month-old mice (n = 3). An 1 mL PBS solution containing bone marrow collected from the tibia and femur was prepared. Tissue debris was removed using a mesh cell screen (5 cm × 5 cm). The separation solution was prepared according to the kit specifications (Tianjin Hao Yang Biological Manufacture Co., Ltd., LZS1100, Tianjin, China); then, 3 mL of 100% cell separation solution, 1.5 mL of 80% cell separation solution, and 1 mL of sample solution were added to the centrifuge tube, which was centrifuged at 1000×g for 30 min. After centrifugation, the cells between the 100% and 80% cell separation solutions were removed. Then, the mixture was centrifuged at 1000×g for 4 min to remove the supernatant, and 200 μL PBS containing 1 μL PE-conjugated anti-mouse Ly6G antibody (Bio-Legend, B281017, San Diego, CA, USA) was added and incubated for 30 min. The total number of cells isolated from the tibia and femur was determined using a hemocytometer, and the variation in neutrophils in the isolated cell samples was determined by flow cytometry (Becton, Dickinson and Company, FACSCanto II, Franklin Lakes, NJ, USA).

2.6. Uptake of SA-modified liposomes

The uptake of SA-modified liposomes by B16/F10 cells, neutrophils, and HL-60 cells was determined using CLSM (ZEISS, ZEISS LSM 800, Oberkochen, Germany) and flow cytometry (Becton, Dickinson and Company). Cells were incubated with SA solution for 12 h, and 1 mL of SA-presaturated HL-60 cells or normal HL-60 and B16/F10 cells suspension (1 × 10^6 cells/mL) was added to 6-well plates containing cell slides and incubated for 4 h at 37 °C in a 5% CO_2 cell incubator. 1 mL of serum-free medium containing SL-Co was added (DOX final concentration: 50 μg/mL; ICG final concentration: 20 μg/mL, 808 nm laser: 3 min) and the cell suspension was further incubated. The medium was removed from the 6-well plates used for the ingestion experiment after 2 h. Then, 500 mL of 4% paraformaldehyde was separately added to the 6-well plate and the cells were stained with DAPI (Dalian Meilun Biological Co., Ltd., MA0128-Jan-14H, Dalian, China) for 10 min (50 μg/mL). The cell slides were then removed and placed upside down on a glass slide with 10 μL of

mounting medium containing anti-fluorescence quenching reagent and observed.

The same processes, for 12 h and 30 min, of adding B16/F10 cells, preparations, laser irradiation, and 200 μL of PBS containing 1 μL FITC-conjugated anti-mouse CRT antibody (eBiosciences, San Diego, CA, USA) to 6-well plates were used for the ICD experiment. The proportion of CRT^+/PI^- cells was determined by flow cytometry. Then, 1 mL of cell medium supernatant was removed, centrifuged at 1000×*g* for 20 min, and the related cytokines were determined using the ATP Test Kit (Quanzhou Ruixin Biological Technology Co., Ltd., Shenzhen, China)and HMGB-1 ELISA Kit (R&D Systems, Minneapolis, MN, USA).

2.7. Tissue distribution of SA-modified liposomes

The skin on the back of 2-, 8-, and 16-month-old mice were depilated, disinfected, and injected with 200 μL of a B16/F10 cell suspension (10^7 cells/mL). When the tumor volumes reached approximately 1000 mm^3, the tumor-bearing mice were divided into three groups: 2-month-old mice injected with SL-DiR (2M-DiR) group, 8-month-old mice injected with SL-DiR (8M-DiR) group, and 16-month-old mice injected with SL-DiR (16M-DiR) group *via* the tail vein (DiR: 1 mg/kg). At 2, 6, 12, and 24 h after the injection, fluorescence images of the 2-, 8-, and 16-month-old mice ($n = 3$) were obtained using a live imaging device. The brain, heart, lung, tumor, spleen, kidney, and liver of all of the mice were dissected and images of the fluorescence were captured.

2.8. Anti-tumor therapy with SA-modified liposomes

The skin of the back of the legs of 2-, 8-, and 16-month-old mice ($n = 24$) was depilated, disinfected, and injected with 200 μL of a B16/F10 cell suspension (10^7 cells/mL). When the tumor volume reached 100 mm^3, the tumor-bearing mice were randomly divided into 12 groups ($n = 6$): 2-month-old mice injected with 5% glucose (2M-Con) group, 2-month-old mice injected with SL-DOX (2M-DOX) group, 2-month-old mice injected with SL-ICG (2M-ICG) group, 2-month-old mice injected with SL-Co (2M-Co) group, 8-month-old mice injected with 5% glucose (8M-Con) group, 8-month-old mice injected with SL-DOX (8M-DOX) group, 8-month-old mice injected with SL-ICG (8M-ICG) group, 8-month-old mice injected with SL-Co (8M-Co) group, 16-month-old mice injected with 5% glucose (16M-Con) group, 16-month-old mice injected with SL-DOX (16M-DOX) group, 16-month-old mice injected with SL-ICG (16M-ICG) group, and 16-month-old mice injected with SL-Co (16M-Co) group. Liposomes were injected into the tail vein 1, 4, and 7 days after grouping (DOX: 5 mg/kg, ICG: 2 mg/kg). At 6 h after administration, the tumor site of each mouse was subjected to 808 nm laser irradiation for 3 min (2 W/cm^2, Zoletil® 50: 50 mg/kg, Beijing You Pet Biotechnology Co., Ltd., Beijing, China), and the temperature variation at the tumor site was observed. The measurements of the body weight and the long and short diameters of the tumors were performed to calculate the tumor volume.

The TDLNs of 2-month-old mice were removed to eliminate ICD induced by photochemotherapy. Mice were randomly divided into three groups ($n = 6$): 2-month-old mice injected with 5% glucose (2M-Sham), 2-month-old mice injected with SL-Co (2M-LN), and 2-month-old mice (no TDLN) injected with SL-Co (2M-No-LN). Consistent with the above administration method, the long and short diameters of the tumors were measured to calculate the tumor volumes.

2.9. Immunofluorescence assays

Immunofluorescence was used to detect enhanced $CD8^+$ T cell infiltration in the tumors. On the 25th day, TDLNs, heart, kidney, thymus, skin, lung, and liver were placed in 4% polymethylene fixation solution and then embedded in paraffin. Ultra-thin sections (5 μm) were generated and stained with H&E (Wuhan Servicebio Biotechnology Co., Ltd., Wuhan, China). The sections were observed under an inverted microscope. Tumors were homogenized, and cytokines in tumor supernatants were assayed by using Enzyme-linked immunosorbent assay (ELISA) kits for interferon-gamma (IFN-γ), tumor necrosis factor-α (TNF-α), IL-10, and IL-2 (eBiosciences, 16MSTE1QPQ, 62SBL6ULPC, E-EL-R0016C, BIJLXURBFW, San Diego, CA, USA). In addition, paraffin sections of the embedded tumors were subjected to TUNEL and immunofluorescence staining ($CD11b^+$ dendritic cells; $CD4^+$ T cells; Neutrophils; $CD8^+$ T cells, Wuhan Servicebio Biotechnology Co., Ltd., Wuhan, China). Paraffin sections of the embedded TDLNs were stained with immunofluorescence probes ($CD4^+$ T cells and $CD8^+$ T cells). All fluorescence-labeled sections were observed under a fluorescence microscope (NIKON CORPORATION, Nikon Eclipse Ti-Sr, Tokyo, Japan). T cells in TDLNs from mice of different ages were separated according to the process described in Subsection 2.5.1, and the variation in $CD8^+$ T cells in TDLNs was determined using flow cytometry ($CD3^+$ T cells, $CD8^+$ T cells).

2.10. Statistical analysis

Data are presented as means ± standard deviation. The IC_{50} and *P* value were determined using SPSS 23.0 software (IBM Corp., IBM SPSS Statistics 23.0, Armonk, NY, USA). One-way ANOVA followed by a post hoc test was used for multiple group comparisons. Independent Samples *t*-test was used for comparisons between two groups. $^*P < 0.05$, $^{**}P < 0.01$, $^{***}P < 0.001$. ns, not significant.

3. Results

3.1. SA-modified DOX and ICG co-loaded liposomes

Immune cells have received widespread attention as drug delivery carriers because of their excellent anti-tumor therapeutic efficacy. SA can combine to the L-selectin on the surface of neutrophils, but SA cannot be modified on the surface of liposomes. Thus, we designed MT-18 with a molecular weight of 561 Da (Supporting Information). We found that the molecular docking energy and interacting amino acid residues of MT-18 were the same as those of SA by Autodock Vina; MT-18 retained the ability of SA to target L-selectin on neutrophils and could be modified on the surface of the liposome using octadecyl (Supporting Information)[27,28]. To obtain SA-modified photosensitive liposomes with uniform particle size and good stability, we prepared SL-DOX, SL-ICG, and SL-Co by thin-film evaporation. The

physical appearance of SL-DOX, SL-ICG, and SL-Co did not change significantly at 4 °C after 20 d (Fig. 1A). The particle sizes of SL-DOX, SL-ICG, and SL-Co were 110−125 nm, and the *Zeta* potential ranged from −10 to −15 mV (Table 1). The results of TEM are consistent with the results of Nicomp-380 dynamic light scattering particle sizer. DOX could interact with sulfate to form an insoluble polymer inside SL-Co and SL-DOX (Fig. 2 B and C). After 808 nm laser irradiation for 3 min, the temperatures of SL-Co and SL-ICG were above 60 °C, but the temperature of SL-DOX did not exceed 30 °C, indicating that SL-DOX had no thermal effect (Fig. 2D). The release of DOX and ICG from SL-Co within 48 h was not significantly different from the release from SL-DOX and SL-ICG (DOX: P value = 0.224, ICG: P value = 0.460). After 808 nm laser irradiation for 3 min, the release of DOX and ICG from La-Co within 48 h was significantly increased (DOX: P value < 0.001, ICG: P value < 0.001). SL-ICG and SL-Co not only had uniform particle sizes and good stability under non-illuminated conditions but also accelerated the release of drugs under 808 nm laser irradiation.

3.2. *SA-mediated photochemotherapy eliminated the immunosenescence-mediated decline in antitumor therapeutic efficacy in 16-month-old mice*

There is an inevitable which influences each other between aging, immunity, and tumors. To explore the relationship between immunosenescence and the antitumor therapeutic efficacy of SA-mediated photochemotherapy, we examined anti-tumor-treated efficacies in 2-, 8-, and 16-month-old tumor-bearing mice. For the SA-mediated non-photochemotherapy group, the tumor volume of 16-month-old mice was significantly larger than that of 8-month-old mice (Glucose: P value < 0.001, DOX: P value < 0.001, ZOL: P value < 0.001), there was not a significant difference in tumor volumes between 2- and 8-month-old mice during anti-tumor treatment (Glucose: P value = 0.151, DOX: P value = 0.911, ZOL: P value = 0.126), indicating that immunosenescence could influence the antitumor therapeutic efficacy in 16-month-old mice (Fig. 2A−C). Mice aged 2-, 8-, and 16-month that were injected with SL-Co exhibited effective inhibition of tumor growth, and the reduction of the anti-tumor therapeutic effect seen previously in 16-month-old mice was not discernible in the 16M-Co group (Fig. 2D). After 59 days, the total survival time of the 16-month-old mice injected with SL-ICG and SL-DOX significantly decreased compared to that of the 8-month-old mice. The total survival times of the 2-, 8-, and 16-month-old mice injected with SL-Co were the same (Fig. 2E). During the first phototherapy treatment, the temperatures of the tumor sites of the 2-, 8-, and 16-month-old mice injected with SL-ICG and SL-Co could reach 48−50 °C, but it took relatively longer for the temperature of the tumor sites in the 16-month-old mice to reach the maximum temperature (Fig. 2F). The TUNEL fluorescence intensity in 8M-DOX was 3.9-times that in 16M-DOX and 1.7-times

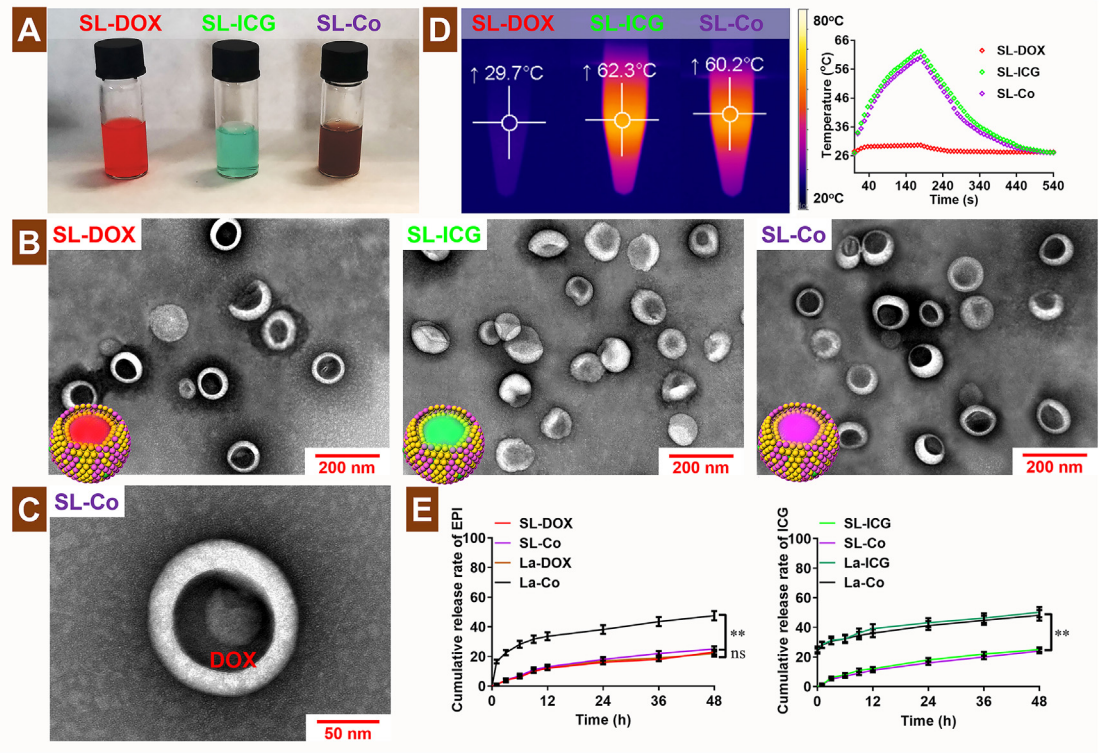

Figure 1 (A) Image of 1 mL of SL-DOX, SL-ICG, and SL-Co placed separately in 2 mL penicillin bottles at 4 °C for 20 days. (B) TEM of SL-DOX, SL-ICG, and SL-Co, scale bar = 200 nm. (C) An insoluble precipitate formed by the interaction of DOX and sulfate in the aqueous phase of SL-Co, scale bar = 50 nm. (D) Thermal images of 200 μL of SL-DOX, SL-ICG, and SL-Co irradiated vertically by 808 nm laser for 3 min (2 W/cm^2), and temperature change curve of the liposomes. (E) Cumulative release curves of SL-DOX, SL-ICG, SL-Co, La-DOX, La-ICG, and La-Co (DOX: 1 mg/mL; ICG: 0.4 mg/mL, n = 3). Data are presented as mean ± SD. **P < 0.01. ns, not significant.

Table 1 Prescription composition, particle size, PDI, zeta potential, and *EE* of liposomes. Data are presented as mean ± SD ($n = 3$).

Liposomes	Drug	Drug/lipid (*w*/*w*)	Composition (*n*/*n*/*n*)	Particle size (nm)	PDI	Zeta potential (mV)	EE (%)
SA-ICG	ICG	3: 20	MT-18/DPPC/ HSPC/CH = 5/30/25/40	109.2 ± 1.4	0.112 ± 0.010	−13.1 ± 1.2	25.6 ± 1.8
SA-DOX	DOX	1: 10	MT-18/DPPC/ HSPC/CH = 5/30/25/40	108.1 ± 1.3	0.109 ± 0.009	−11.2 ± 1.2	94.8 ± 2.1
SA-Co	ICG, DOX	3: 20, 1: 10	MT-18/DPPC/ HSPC/CH = 5/30/25/40	107.4 ± 1.6	0.123 ± 0.011	−12.6 ± 1.3	24.5 ± 1.6, 87.7 ± 2.6

PDI, polydispersity index; EE, encapsulation efficiency; ICG, indocyanine green; DOX, doxorubicin; SL-ICG, SA-modified ICG-loaded liposomes; SL-DOX, SA-modified DOX-loaded liposomes; SL-Co, SA-modified ICG and DOX co-loaded liposomes; MT-18, methyl sialic acid-octadecanoic acid; DPPC, dipalmitoyl phosphatidylcholine; HSPC, hydrogenated soybean phosphotidylcholine; CH, cholesterol.

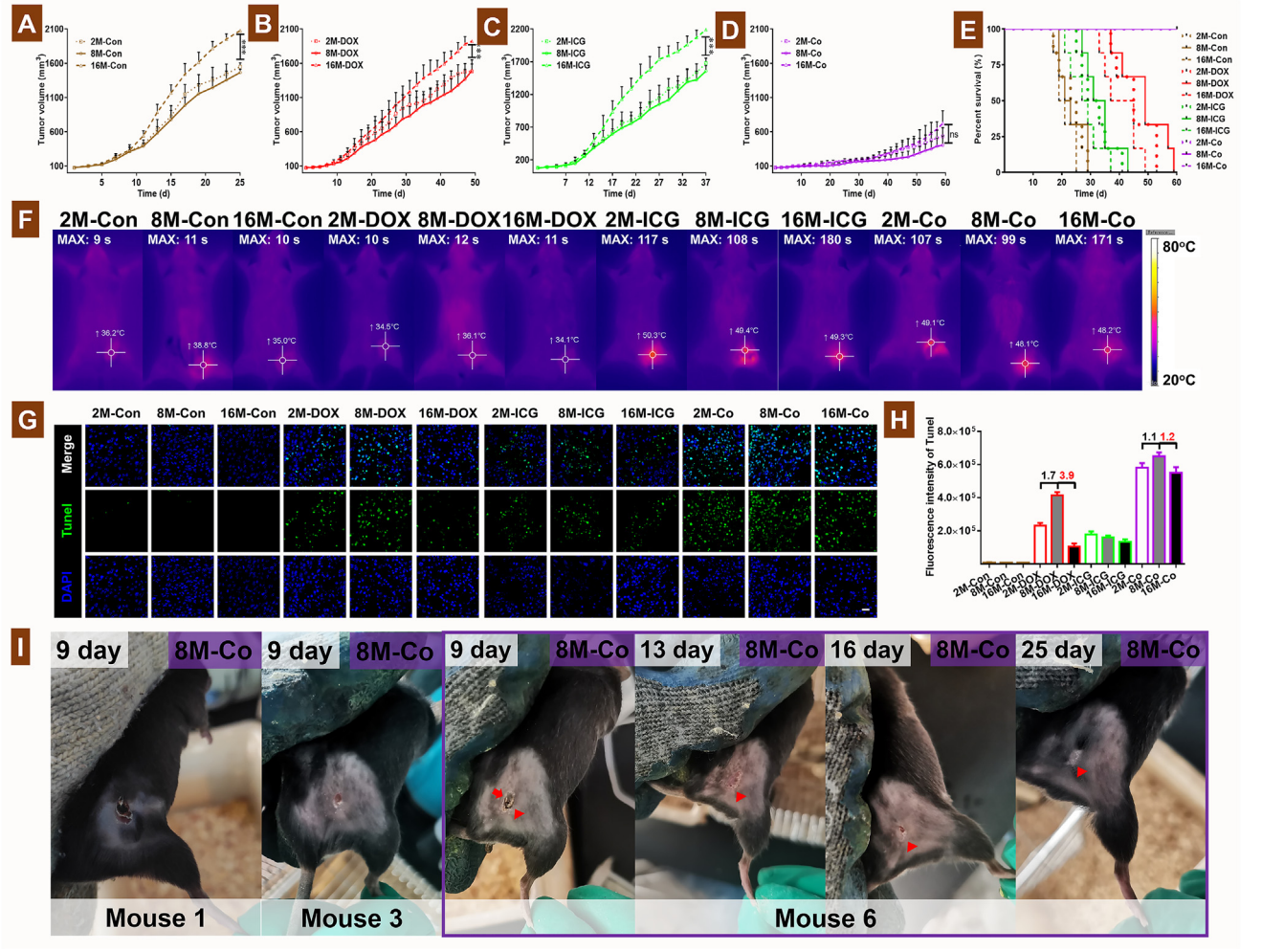

Figure 2 SA-mediated photochemotherapy eliminates the decline of antitumor therapeutic efficacy caused by immunosenescence. Tail vein injection of mice of different ages, (A) tumor volume of mice injected with 5% Glu, (B) tumor volume of mice injected with SL-DOX, (C) tumor volume of mice injected with SL-ICG, (D) tumor volume of mice injected with SL-Co, (E) percent survival after 59 d of treatment ($n = 6$, death, the shortest tumor dimension reached 1.5 cm, and the volume reached more than 2000 mm^3, treatment was judged to be ineffective). (F) 2-, 8-, and 16-month-old mice were injected with liposomes after 6 h (DOX: 5 mg/kg, ICG: 2 mg/kg), and the highest temperature of tumor site for the indicated durations of 808 nm laser irradiation are specified. (G) TUNEL fluorescence section of tumor site in each treated group (apoptotic cells: green). (H) Fluorescence intensity of TUNEL in 200 μm × 200 μm image was measured using ImageJ ($n = 3$, scale bar = 20 μm). (I) The tumors of mice in the 8M-Co group became crusted (red arrow) and regressed (red triangle). Data are presented as mean ± SD. ***$P < 0.001$. ns, not significant.

that in 2M-DOX. The TUNEL fluorescence intensity in 8M-Co was 1.2-times that in 16M-Co and 1.1-times that in 2M-Co, indicating non-significant differences between them (Fig. 2G and H). The results of the TUNEL stained sections were consistent with the tumor volume growth curves, indicating that SA-mediated photochemotherapy eliminated the decline in anti-tumor therapeutic efficacy in the 16-month-old mice. Fifty percent of the tumors in the 8M-Co group became scabbed and regressed by SA-mediated photochemotherapy, and there were no signs of recurrence within 59 days (Fig. 2I).

3.3. *Decline in CD8$^+$ T cells functioning in 16-month-old mice is caused by immunosenescence*

Immunosenescence is due to degeneration of the thymus[7,29]. Degeneration of the thymus influences the phenotype and function of T cells, which can influence the body's immune system[9]. To document the relationship between aging and immunity, immune tissue sections, and T lymphocytes of 2-, 8-, and 16-month-old mice were analyzed. Functional atrophy of the thymus occurred in 16-month-old mice (Fig. 3A), and the cell density in the lymph nodes of 8-month-old mice was significantly higher than that of 2- and 16-month-old mice (Fig. 3B). The variation in the number of T lymphocytes in the thymus and lymph nodes accurately reflects the variation in the immune system of 2-, 8-, and 16-month-old mice. The total cell number and the ratio of CD3$^+$ T cells in the thymus of 16-month-old mice were lower than those of 2- and 8-month-old mice (Fig. 3 C and D). The number of CD3$^+$ T cells in the thymus of 8-month-old mice was 6.38-times that of 16-month-old mice (Fig. 3E). The total cell number and the ratio of CD3$^+$CD8$^+$ T cells in the lymph nodes of 16-month-old mice were lower than those of the 8-month-old mice (2.89-times, Fig. 3F and G). The numbers of T cells CD8$^+$ and CD3$^+$ T cells in the lymph nodes of 8-month-old mice were 4.22- and 3.86-times that of 16-month-old mice, respectively (Fig. 3 H and I). The numbers of T cells in the thymus and lymph nodes were, however, the same. Thus, it can be concluded that immunosenescence occurred in 16-month-old mice.

3.4. *Neutrophils-mediated delivery of SA-dependent photochemotherapy to target tumors*

Neutrophils also undergo a series of degenerative changes in their function and number, and their self-regulatory, phagocytic, and antigen-presenting capabilities are also significantly weakened[7]. The ratio of neutrophils in the tibia and femur of 16-month-old mice was lower than that in 2- and 8-month-old mice (Fig. 4A). The total cell number and the number of neutrophils in the tibia and femur of 8-month-old mice were 1.77-, and 2.71-times, respectively, that of 16-month-old mice (Fig. 4B and C). The anti-tumor effects of SA-modified liposomes involve three stages: phagocytosis, transport, and effectuation[17]. We used SA-presaturated HL-60 cells and SA-modified liposomes to explore the relationship between the neutrophils drug delivery system and immunosenescence. After neutrophils and HL-60 cells were incubated with SA (10 mol/L) for 12 h, we found that the uptake capability of SA-presaturated cells was lower than that of normal cells. The binding of free SA to the L-selectin of neutrophils inhibits the uptake of SL-Co, and it can be concluded that tumor delivery of drugs by liposomes is mediated by neutrophils (Fig. 4D). After injection with SL-DiR, the fluorescence intensity of DiR in the tumors of 2-, 8-, and 16-month-old mice reached the highest value at 6 h. The fluorescence intensity of DiR in the brain, heart, lung, spleen, kidney, and tumors of 2-, 8-, and 16-month-old mice was not different at 2, 6, 12, and 24 h. DiR accumulation in the tumors of 16-month-old mice was significantly lower than that in 8-month-old mice at 6 and 12 h (6 h: P value < 0.001, 12 h: P value < 0.001), and the amount of DiR

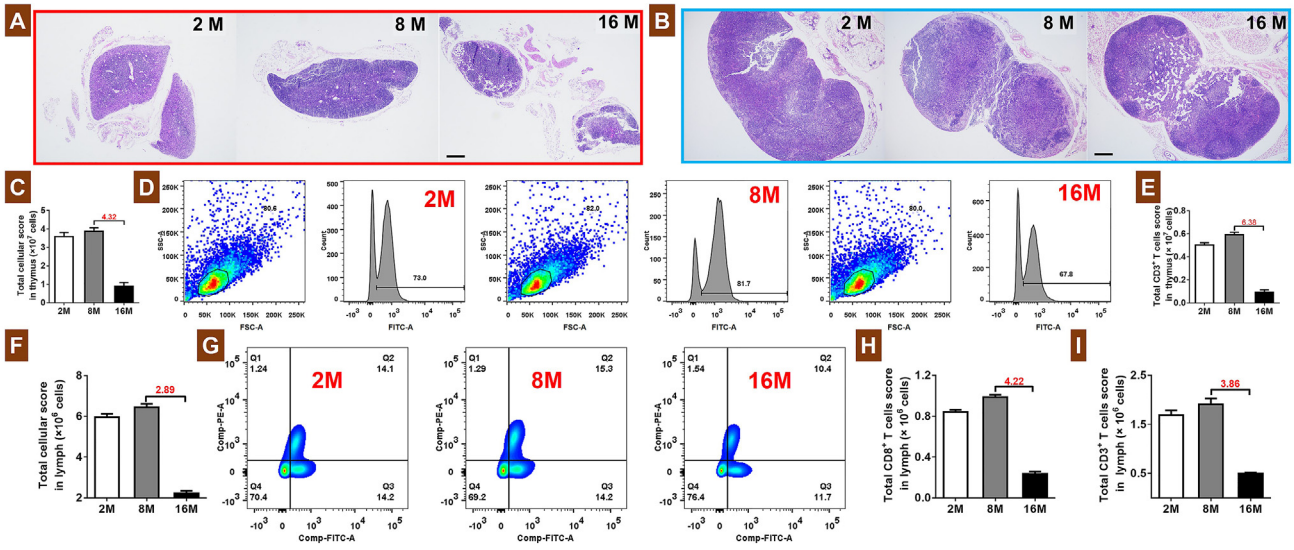

Figure 3 Aging of CD8$^+$ T cells of 16-month-old mice caused by immunosenescence. (A) Thymus, and (B) TDLNs of 2-, 8-, and 16-month-old mice, scale bar = 200 μm. (C) Total cell number, (D) ratio of CD3$^+$ T cells, (E) and a total number of CD3$^+$ T cells in thymus, n = 3. (F) Total cell number, (G) ratio of CD3$^+$CD8$^+$ T cells, (H) a total number of CD8$^+$ T cells, (I) and a total number of CD3$^+$ T cells in TDLNs (CD8$^+$ T cells were labeled with PE-CD8 antibody; CD3$^+$ T cells were labeled with FITC-CD3 antibody, n = 3). Data are presented as mean ± SD.

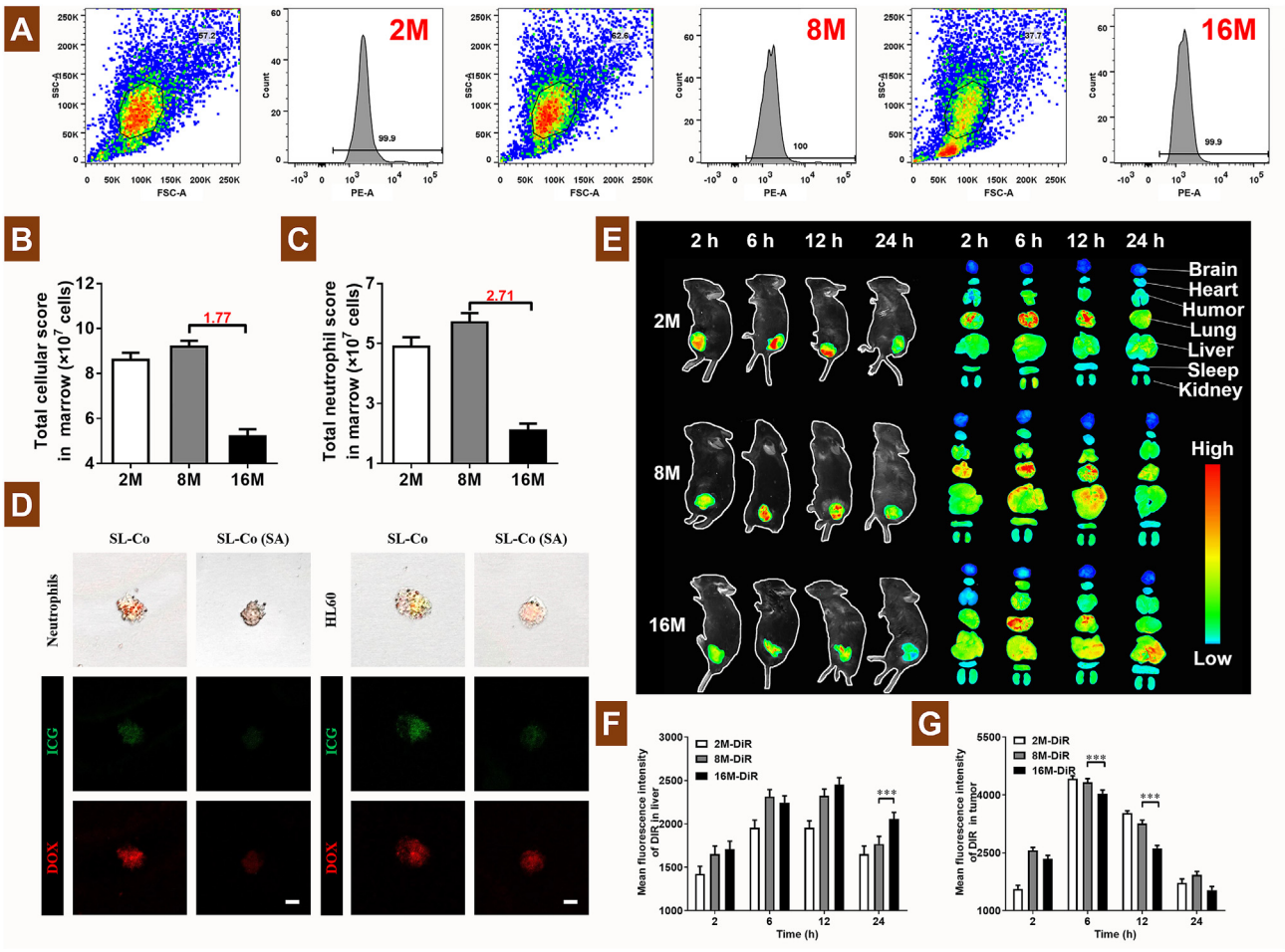

Figure 4 Neutrophil-mediated drug delivery by SA-modified liposomes to target tumors. (A) Purity of neutrophils, (B) total cell number, and (C) total number of neutrophils in the femur and tibia (neutrophils were labeled with PE-Ly6G antibody, $n = 3$). (D) SA-presaturated HL-60 cells and normal HL-60 cells were incubated with SL-Co for 2 h; images of intracellular DOX (red) and ICG (green) fluorescence are shown (scale bar = 10 μm). (E) Tail vein injection of SL-DiR in 2-, 8-,16-month-old mice (DiR: 1 mg/kg, $n = 3$); fluorescence distribution image was shown. (F) Fluorescence intensity of DiR in liver and (G) tumor of the mice at 2, 6, 12, and 24 h. Data are presented as mean ± SD. ***$P < 0.001$.

accumulation in the liver of 16-month-old mice was significantly higher than that in 8-month-old mice at 24 h (P value < 0.001). Furthermore, the amount of DiR accumulation in tumors and livers of 8- and 2-month-old mice was not different at 2, 6, 12, and 24 h (Fig. 4E–G). The above results indicate that neutrophils delivered the SL-DiR to the tumor sites, and neutrophil senescence in the 16-month-old mice affected liposome accumulation in the tumors.

3.5. SA-mediated photochemotherapy enhanced immunogenic death of B16/F10 cells

Immunogenic death of tumor cells generated a series of damage-associated molecular patterns (DAMPs) (Fig. 5A)[30]. To verify that SA-mediated photochemotherapy enhanced immunogenic death of B16/F10 cells, surgical removal of TDLNs from 2-month-old mice was performed to generate a no-immune-response mouse model. For the SL-Co group, the tumor volume of the mice with no TDLNs was significantly larger than that of normal mice (P value < 0.001), indicating that SA-mediated photochemotherapy enhanced the infiltration of immune cells from TDLNs into the tumor (Fig. 5B). In the CCK8 test, the IC_{50} value of La-Co was lower than those of La-ICG and La-DOX groups, and CI < 1 (Table 2). There was a greater accumulation of DOX in B16/F10 cells in the La-Co group than that in the SL-Co group, and there was no difference in ICG uptake between the SL-Co and the SL-ICG groups (Fig. 5C). In the *in vitro* ICD experiment, the ratio of CRT^+/PI^-, release of ATP, and secretion of HMGB-1 in the La-Co group were significantly higher than those in the other groups (Fig. 5D). For non-photochemotherapy, the number of dendritic cells in the tumors of the 16-month-old mice was lower than that in the 2- and 8-month-old mice. SA-mediated photochemotherapy enhanced dendritic cell infiltration into the tumors of the 16-month-old mice (Fig. 5E). SA-mediated photochemotherapy converted light energy into heat energy to accelerate the release of DOX, thereby increasing the toxicity of DOX and enhancing B16/F10 cell ICD.

3.6. SA-mediated photochemotherapy enhanced the $CD8^+$ T cells tumor infiltration in 16-month-old mice

The ultimate goal of anti-tumor therapy is to eliminate cancer cells, and enhancing the infiltration of immune cells into the tumor is key to achieving this[31,32]. Cytokines (TNF-α, IFN-γ, IL-2, and

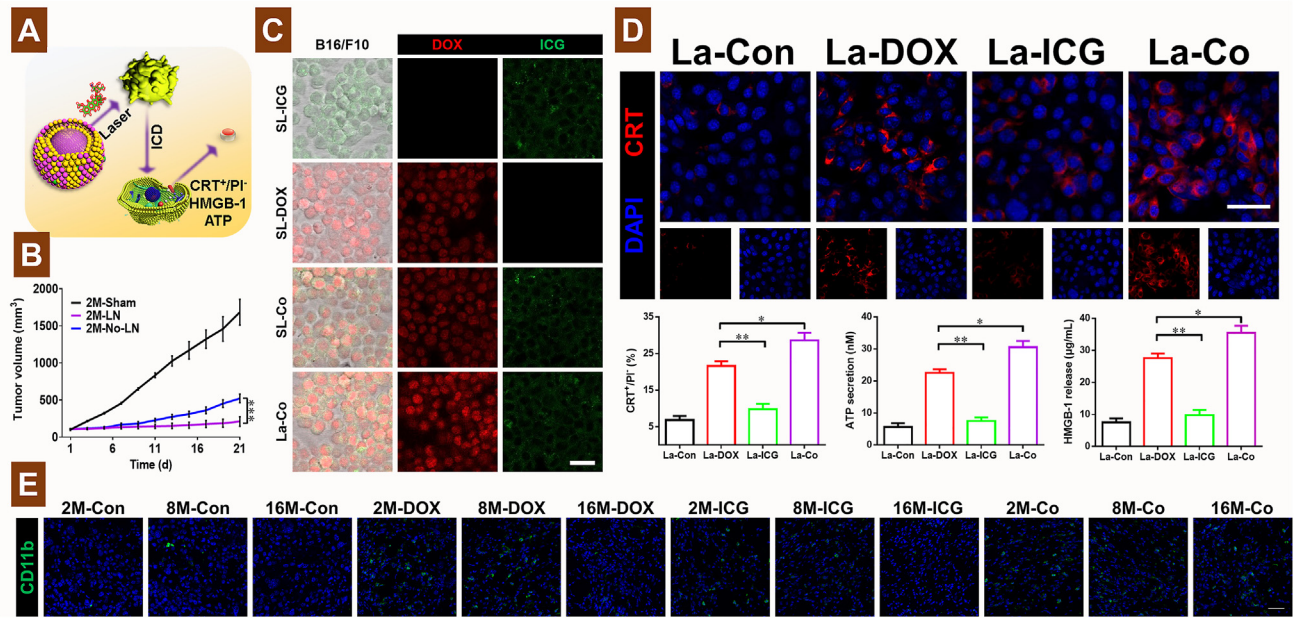

Figure 5 SA-mediated photochemotherapy enhanced immunogenic death of B16/F10 cells. (A) ICD of tumor cells. (B) Changes in tumor volume of mice without TDLNs and normal mice during the 21 d of anti-tumor treatment. (C) B16/F10 cells were incubated with the liposomes for 2 h; confocal fluorescence images of non-irradiated and irradiated B16/F10 cells are shown (Red: DOX; Green: ICG, La-Co: 808 nm laser irradiated for 3 min, scale bar = 30 μm). (D) B16/F10 cells were incubated with liposomes for 12 h, confocal fluorescence image of B16/F10 cells (red: CRT, blue: DAPI) was taken and ratio of CRT^+/PI^- in B16/F10 cells (n = 3, scale bar = 30 μm) was measure. Changes in the levels of ATP and HMGB-1 were determined by ATP and HMGB-1 kits. (E) Fluorescence images of dendritic cells (green) in tumor of mice in different treated groups (scale bar = 40 μm). Data are presented as mean ± SD. $^*P < 0.05$, $^{**}P < 0.01$, $^{***}P < 0.001$.

IL-10) activate immune cells, enhance their infiltration into tumors, and regulate the immune response. The concentrations of TNF-α, IFN-γ, IL-2, and IL-10 in the tumors of 2-, 8-, and 16-month-old mice injected with SL-ICG and 5% glucose were significantly lower than those in mice injected with SL-DOX or SL-Co. The concentrations of TNF-α, IFN-γ, IL-2, and IL-10 in the tumors of 8-month-old mice were higher than those of 16-month-old mice, and SL-Co could narrow differences in the concentration of cytokines between 2-, 8-, and 16-month-old mice (Fig. 6A and B). The proportion of $CD3^+CD8^+$ T cells in TDLNs of 2-, 8-, and 16-month-old mice injected with SL-ICG and 5% glucose was lower compared to those injected with SL-DOX or SL-Co (Fig. 6C). The total cell number, the number of $CD3^+$ T cells, and the number of $CD3^+CD8^+$ T cells in the TDLNs of the 8-month-old mice were higher than those of the 16-month-old mice (Fig. 6D−F). There was not a significant difference in the number of $CD4^+$ T cells in the TDLNs of 2-, 8-, and 16-month-old mice injected with the same preparation (Fig. 7A and B). The number of $CD8^+$ T cells in the TDLNs of the 8M-DOX group was 2.7-times that of the 16M-DOX group, and the number of $CD8^+$ T cells in the TDLNs of the 8M-Co group was 1.4-times that of the 16M-Co group. The number of $CD8^+$ T cells in the TDLNs of the 8-month-old mice was significantly higher than that of the 16-month-old mice (Fig. 7C). The change in the trend of $CD4^+$ and $CD8^+$ T cells in the thymus was the same as that in the TDLNs (Fig. 7D−F). Therefore, it would appear that photochemotherapy can increase the release of cytokines that induce T cell activation in the tumor and enhance tumor infiltration of $CD8^+$ T cells in the TDLNs of immunosenescent mice.

Table 2 IC_{50} value and CI after 48 h of incubation of B16/F10 cells with liposomes. Data are presented as mean ± SD (n = 6).

Parameter	SL-ICG	SL-DOX	SL-Co
IC_{50} (μg/mL)	26.9 ± 0.5	15.9 ± 0.3	6.4 ± 0.3
CI	−	−	0.7 ± 0.1

CI, combination index; IC_{50}, half maximal inhibitory concentration; SL-ICG, SA-modified ICG-loaded liposomes; SL-DOX, SA-modified DOX-loaded liposomes; SL-Co, SA-modified ICG and DOX co-loaded liposomes; −, not applicable.

3.7. *SA-mediated photochemotherapy reduced tumor recurrence and metastasis*

As long as tumor cells are still present, recurrence and metastasis will remain the main factors that threaten patient survival. In the wound-healing assay, there was not a significant difference in the migration ability of tumor cells in the control *versus* La-ICG groups (12 h: P value = 0.074, 24 h: P value = 0.158), and the migration ability of B16/F10 cells in the La-Co group was significantly less than that in the La-ICG group at 12 and 24 h (12 h: P value < 0.001, 24 h: P value < 0.001, Fig. 8A and B). DOX effectively reduced the migration ability of tumor cells, and its inhibitory effect on tumor cell migration was greater than that of ICG. Only the 16-month-old mice injected with 5% glucose and SL-ICG exhibited lung and liver metastases of the tumor cells (Fig. 8C). The tumor sites of mice formed scabs in 2M-ICG, 8M-ICG, and 16M-ICG groups during the treatment. We found that the tumor recurrence in situ after the administration was stopped, and the tumor recurrence was the most serious in 16-month-old

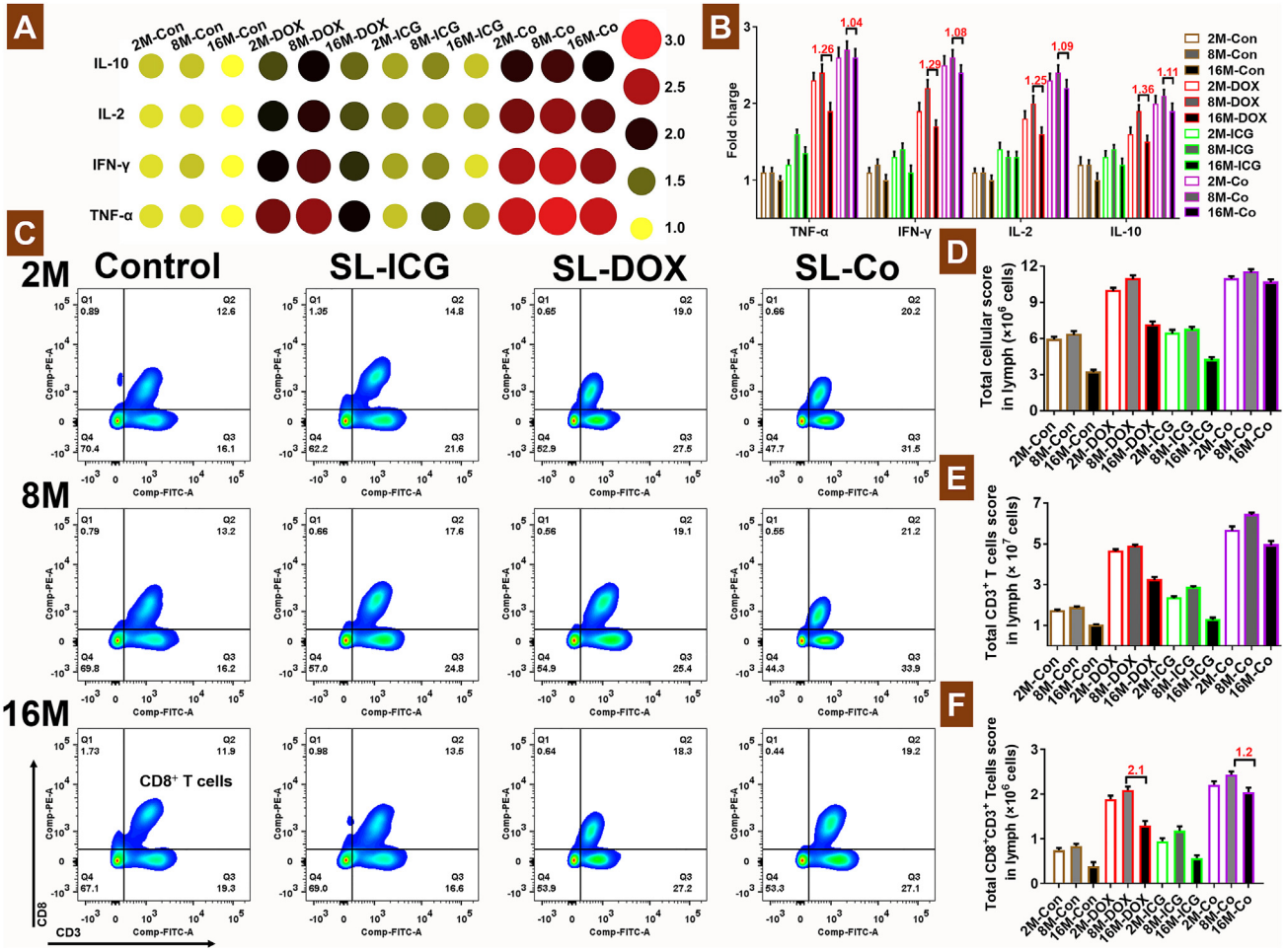

Figure 6 Changes in the levels of cytokines in tumors and the number of T cells in TDLNs of mice in each treated group. (A, B) The changes in cytokine levels in the tumors (1 cm × 1 cm × 1 cm) in each treated group were determined by IFN-γ, TNF-α, IL-10, and IL-2 ELISA kits. Taking the concentration of each cytokine in the tumors of 16M-Con as the control group, the changes in the concentration for the other treated groups were calculated ($n = 3$). (C) The changes in the number of $CD3^+CD8^+$ T cells in TDLNs in each treated group. (D) Total cell number, (E) total $CD3^+$ T cell number, and (F) total $CD3^+CD8^+$ T cell number in lymph nodes ($n = 3$). Data are presented as mean ± SD.

mice (Fig. 8D). During treatment, T cells senescence enhanced the metastasis and recurrence of tumors, and the decrease in the number of T cells in the 16-month-old mice led to a decrease in the therapeutic effect in the SL-ICG group, leading to metastasis of tumors in mice in the 16M-ICG group. There was no obvious pathological damage to the heart, thymus, kidney, skin, or TDLNs in each treated group, indicating that the SA-modified liposomes did not damage non-cancerous tissues (Fig. 8E).

4. Discussion

In this study, SA-mediated photochemotherapy successfully reversed the immunosenescence-mediated decline in anti-tumor therapeutic effects in 16-month-old mice caused by the light-heat-chemical-immunity conversion. Aging causes immune organs to gradually become functionally degraded, and the number of immune cells in the human body decreases, thereby increasing the risk of disease and the difficulty of treating disease (especially immune-related diseases)[33]. The aging of the thymus, which is the main organ involved in T cell maturation, directly affects the number of mature T cells in the body and indirectly affects the type and quantity of T cells in TDLNs[9]. The thymus and lymph nodes of 2-, 8-, and 16-month-old mice were used to probe for the occurrence of immunosenescence in 16-month-old mice. Neutrophils undergo a series of degenerative changes in their function and number. The number of neutrophils in the 16-month-old mice decreased significantly, and neutrophils-mediated drug delivery was also affected by immunosenescence. However, SA-mediated photochemotherapy increased the infiltration of neutrophils into tumors.

TDLNs have recently been shown to be the key to generating immune responses and enhancing T cell infiltration into tumors. Continuous induction of effective anticancer immune responses is related to the production of activated T cells in TDLNs[10,34]. Studies have shown that the solid stress of the tumor prevents T lymphocytes from entering the tumor, and the number of T cells in the lymph nodes is not affected by the tumor[35,36]. Atrophy of the thymus in 16-month-old mice results in a decrease in the number and tumor infiltration capacity of T cells in TDLNs. Phototherapy reduces the number of tumor cells, changes the solid pressure of the tumor in the TDLNs, and enhances neutrophil infiltration into the tumor. However, phototherapy could not charge the number of

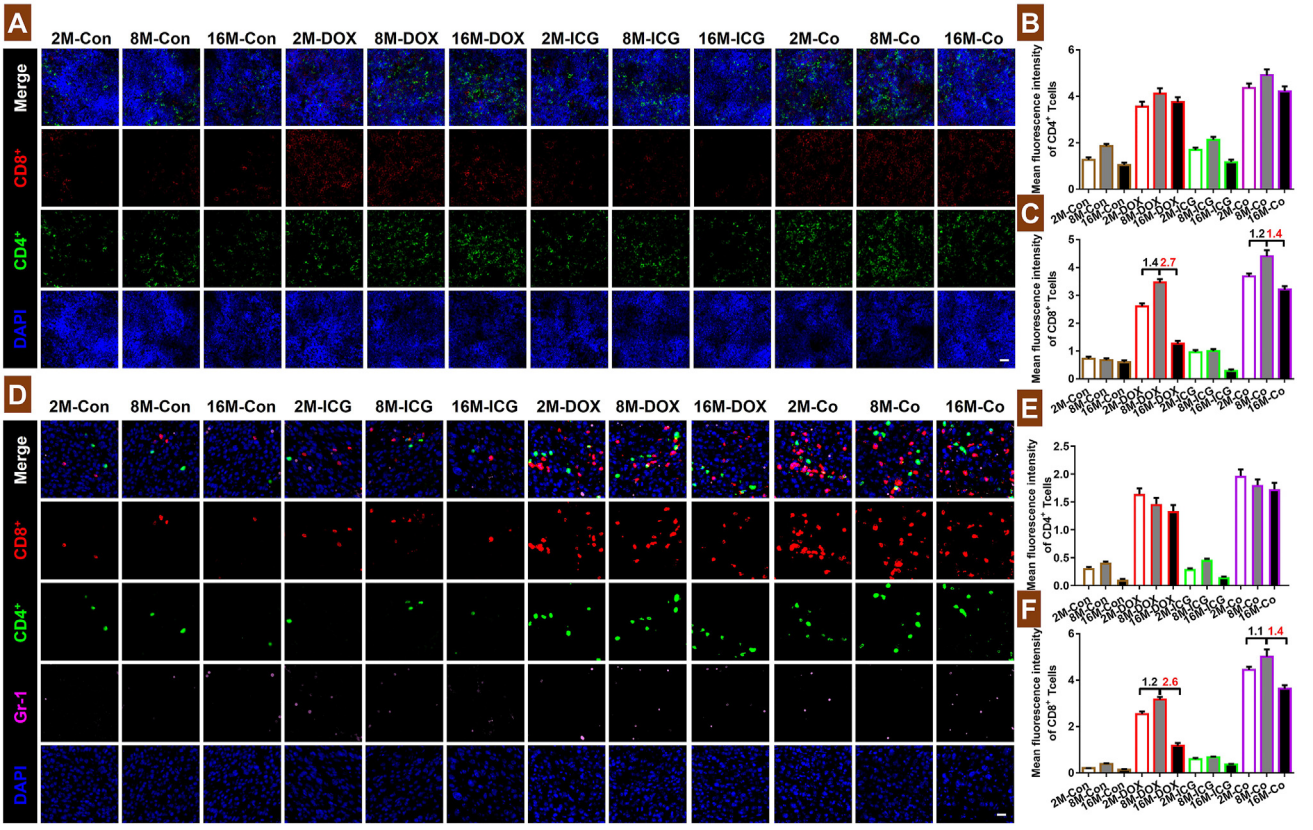

Figure 7 Fluorescence images of sections of TDLNs and tumors in mice in the different treated groups. (A) Fluorescence images of TDLNs of mice in different treated groups; ImageJ was used to measure the fluorescence intensity of (B) $CD4^+$ T cells and (C) $CD8^+$ T cells in 200 μm × 200 μm pictures (red: CD8, green: CD4, blue: DAPI, $n = 3$, scale bar = 20 μm). (D) Fluorescence images of tumors in the different treated groups. ImageJ was used to measure the fluorescence intensity of (E) $CD4^+$ T cells and (F) $CD8^+$ T cells in 200 μm × 200 μm pictures (red: CD8, green: CD4, pink: Gr-1, blue: DAPI, $n = 3$, scale bar = 20 μm). Data are presented as mean ± SD.

T cells and improve the anti-tumor therapy effect in 16-month-old mice, leading to different degrees of recurrence and metastasis of tumors in 16-month-old mice. Chemotherapy regulates tumor-associated immune cells, downregulates tumor-associated macrophage-mediated immunosuppression, induces immunogenic death of tumor cells, enhances $CD8^+$ T cells infiltration into tumors, and transforms immunosuppressive cold tumors into immune-infiltrating hot tumors[37–39]. However, chemotherapy could not improve the efficacy of neutrophil-mediated drug delivery in 16-month-old mice. Unilateral enhancement of drug delivery or improvement of anti-tumor therapy cannot solve the problem of reduced therapeutic effects caused by immunosenescence[40].

As the understanding of tumor cells, tumor microenvironment, and their interaction with the host immune system continues to deepen, the research and development of strategies for anti-tumor therapy continue to change, and the effect of combined administration of an increasing number of new drugs in the early stages of tumor development is now being explored[22,41]. Compared with a single anti-tumor-treated strategy, the combined use of multiple administration strategies can break down the barriers of tumor immunosuppression by non-overlapping mechanisms, increase the number of T lymphocytes infiltrating tumors, and improve anti-tumor therapeutic efficacy. It can reduce the side effects of chemotherapy, prevent the accumulation of drugs in non-cancerous tissues, improve the survival status of patients, and achieve the therapeutic effect of "1 + 1 > 2"[42,43]. During treatment, the accumulation of preparations in the tumor cannot be increased. With increasing age, immunosenescence and changes in the physiological environment of the body profoundly affect the treatment of traditional photochemotherapy[15]. For SA-mediated Photochemotherapy, SA-modified liposomes were targeted to tumors through a neutrophil drug delivery system, and the delivery efficiency of SA-modified liposomes was determined by neutrophils. Photochemotherapy inhibited the growth and migration ability of tumor cells, promoted the presentation of tumor cell antigens, and enhanced neutrophils and T cells infiltration into the tumor. The mutual reinforcement of SA and photochemotherapy have been used to cure tumors.

5. Conclusions

The immune system is important for the distribution of NPs *in vivo*; thus, immunosenescence can have a substantial influence on the anti-tumor therapeutic efficacy of NPs. This study showed that the number of $CD8^+$ T cells and neutrophils in 16-month-old mice significantly decreased, 16-month-old mice exhibited

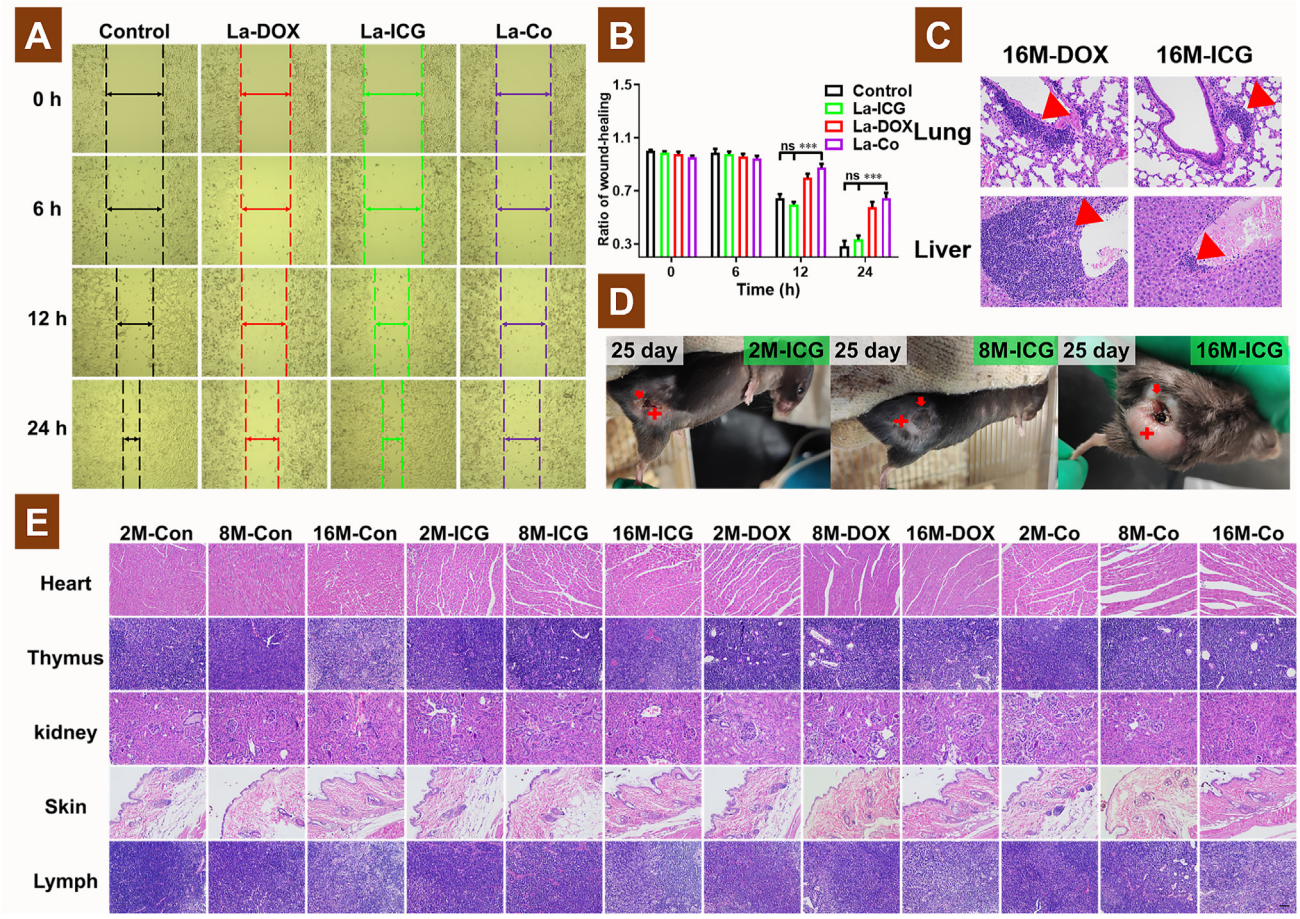

Figure 8 (A) Changes in migration ability of cancer cells; B16/F10 cells were incubated with serum-free medium containing laser irradiated liposomes (DOX final concentration: 50 μg/mL; ICG final concentration: 20 μg/mL, 2 W/cm^2), and was imaged using an inverted microscope at 0, 6, 12, and 24 h. (B) The width of the cell-free area was measured by ImageJ. (C, D) The 25th day after tail vein injection of 2-, 8-, and 16-month-old mice with the liposomes (DOX: 5 mg/mL, ICG: 2 mg/mL, 3 injections), the tumor recurrence of mice in situ and metastasis (red). Scale bar = 50 μm. (E) The dissected heart, thymus, kidney, skin, and TDLNs were paraffin-embedded and sectioned, scale bar = 50 μm. Data are presented as mean ± SD. ***$P < 0.001$. ns, not significant.

immunosenescence, and the immune system of 8-month-old mice was stronger than that of 2-month-old mice. SL-ICG enhanced neutrophils tumor infiltration and specific cytotoxic cells at the tumor site (even scab formation). However, aging of T cells leads to extensive metastasis and the recurrence of tumors, and we noted a significant difference in the treated efficacy in mice of different ages. Regarding the administration of SL-DOX, chemotherapy with this drug-induced ICD in tumor cells and enhanced tumor infiltration by $CD8^+$ T cells. However, neutrophil aging significantly reduced the efficacy of antitumor therapy in 16-month-old mice. Regarding the administration of SL-Co, its therapeutic effect could simultaneously enhance the infiltration of $CD8^+$ T cells and neutrophils into the tumor, increase the accumulation of drugs at the tumor site, improve the effect of antitumor therapy, and eliminate the decline in anti-tumor therapeutic efficacy in 16-month-old mice caused by immunosenescence.

Acknowledgments

This work was supported by the National Natural Science Foundation of China (Grant Nos. 81973271, 81703456, and 81573375) and the Career Development Plan for Young and Middle-aged Teachers of Shenyang Pharmaceutical University (ZQN2021009, China).

Author contributions

Dezhi Sui contributed equally in the design of the study and writing of this manuscript. Yanzhi Song started the project and was joined later with Changzhi Li in the design and execution of majority of the experiments. Yihui Deng assisted in the design and performance of membrane fusion studies and with Xueying Tang. Junqiang Ding assisted with experimental design. Qiongfen Yang, and Zhaowei Qi assisted with rearing mice. Xinrong Liu provided reagents. All authors read and approved the manuscript. Dezhi Sui and Yanzhi Song is involved in overall project design and manuscript preparation. All of the authors have read and approved the final manuscript.

Conflicts of interest

The authors have no conflicts of interest to declare.

Appendix A. Supporting information

Supporting data to this article can be found online at https://doi.org/10.1016/j.apsb.2022.06.005.

References

1. GAYAC Collaborators. The global burden of adolescent and young adult cancer in 2019: a systematic analysis for the Global Burden of Disease Study 2019. *Lancet Oncol* 2021;**23**:27−52.
2. Andrew MK, McElhaney JE. Age and frailty in COVID-19 vaccine development. *Lancet* 2020;**396**:1942−4.
3. Bartleson JM, Radenkovic D, Covarrubias AJ, Furman D, Winer DA, Verdin E. SARS-CoV-2, COVID-19 and the aging immune system. *Nat Aging* 2021;**1**:769−82.
4. Tamas F, Gilles DMWJ, Anis L. The role of immunosenescence in the development of age-related diseases. *Rev Invest Clin* 2016;**68**:84−91.
5. Aw D, Silva AB, Palmer DB. Immunosenescence: emerging challenges for an ageing population. *Immunology* 2007;**120**:435−6.
6. Pawelec G. Age and immunity: what is "immunosenescence". *Exp Gerontol* 2018;**105**:4−9.
7. Arsun BHSS, Ranjan S, Luigi F. Human T cell immunosenescence and inflammation in aging. *J Leukoc Biol* 2017;**102**:977−88.
8. Carrasco E, Heras MMGDL, Rodríguez EG, Micó GD, Aranda JF, Mittelbrunn M. The role of T cells in age-related diseases. *Nat Rev Immunol* 2021;**22**:97−111.
9. Maria M, Guido K. Hallmarks of T cell aging. *Nat Immunol* 2021;**22**:687−98.
10. Fear VS, Forbe CA, Neeve SA, Fisher SA, Chee J, Waithman J, et al. Tumour draining lymph node-generated CD8 T cells play a role in controlling lung metastases after a primary tumour is removed but not when adjuvant immunotherapy is used. *Cancer Immunol Immunother* 2021;**70**:3259.
11. Fulop T, Kotb R, Fortin CF, Pawelec G, Angelis FD, Larbi A. Potential role of immunosenescence in cancer development. *Ann N Y Acad Sci* 2010;**1197**:158−65.
12. Yajas S, Akanksha VRMA, Jessica W, Bhavneet B, Sebastian GMJ, Olivier E. Pan-cancer analysis reveals molecular patterns associated with age. *Cell Rep* 2021;**37**:110100.
13. Lian JY, Yue Y, Yu WN, Zhang Y. Immunosenescence: a key player in cancer development. *J Hematol Oncol* 2020;**13**:151.
14. Perrie Y, Badhan RKS, Kirby DJ, Lowry D, Ar Mohammed D Ouyang. The impact of ageing on the barriers to drug delivery. *J Contr Release* 2012;**161**:389−98.
15. Andriyanov AV, Portnoy E, Koren E, Inesa S, Eyal S, Goldberg SN, et al. Therapeutic efficacy of combined PEGylated liposomal doxorubicin and radiofrequency ablation: comparing single and combined therapy in young and old mice. *J Contr Release* 2017;**257**:2−9.
16. Wang S, Lai XX, Li C, Chen M, Hu M, Liu XR, et al. Sialic acid-conjugate modified doxorubicin nanoplatform for treating neutrophil-related inflammation. *J Contr Release* 2021;**337**:612−27.
17. Ding JQ, Zhao D, Hu YW, Liu MQ, Liu XR, Zhang BW, et al. Terminating the renewal of tumor-associated macrophages: a sialic acid-based targeted delivery strategy for cancer immunotherapy. *Int J Pharm* 2019;**571**:118706.
18. She ZN, Zhang T, Wang XL, Li X, Song YZ, Cheng XB, et al. The anticancer efficacy of pixantrone-loaded liposomes decorated with sialic acid−octadecylamine conjugate. *Biomaterials* 2014;**35**:5216−25.
19. Qiu QJ, Li C, Yan XY, Zhang HX, Luo X, Gao X, et al. Photodynamic/photothermal therapy enhances neutrophil-mediated ibrutinib tumor delivery for potent tumor immunotherapy: more than one plus one? *Biomaterials* 2021;**269**:120652.
20. Li C, Qiu QJ, Gao X, Yan XY, Fan CZ, Luo X, et al. Sialic acid conjugate-modified liposomal platform modulates immunosuppressive tumor microenvironment in multiple ways for improved immune checkpoint blockade therapy. *J Contr Release* 2021;**337**:393−406.
21. Qiu QJ, Li C, Song YZ, Shi T, Luo X, Zhang HX, et al. Targeted delivery of ibrutinib to tumor-associated macrophages by sialic acid-stearic acid conjugate modified nanocomplexes for cancer immunotherapy. *Acta Biomater* 2019;**92**:184−95.
22. Sui DZ, Tang XY, Ding JQ, Wang Y, Qin Y, Zhang N, et al. Sequential administration of sialic acid-modified liposomes as carriers for epirubicin and zoledronate elicit stronger antitumor effects with reduced toxicity. *Int J Pharm* 2021;**602**:120552.
23. Ding JQ, Sui DZ, Liu MQ, Su YQ, Wang Y, Liu MY, et al. Sialic acid conjugate-modified liposomes enable tumor homing of epirubicin *via* neutrophil/monocyte infiltration for tumor therapy. *Acta Biomater* 2021;**134**:702−15.
24. Wang S, Lai XX, Deng YH, Song YZ. Correlation between mouse age and human age in anti-tumor research: significance and method establishment. *Life Sci* 2020;**242**:117242.
25. Has C, Sunthar P. A comprehensive review on recent preparation techniques of liposomes. *J Liposome Res* 2019;**30**:3365.
26. Wvd Broeck, Derore A, Simoens P. Anatomy and nomenclature of murine lymph nodes: descriptive study and nomenclatory standardization in BALB/cAnNCrl mice. *J Immunol Methods* 2006;**312**:12−9.
27. Stefanie W, Jens D, Vf Ardeschir, Rudolf T, Wolfram S, Haydar B. Reducing macro- and microheterogeneity of N-glycans enables the crystal structure of the lectin and EGF-like domains of human L-Selectin to be solved at 1.9 Å resolution. *Chembiochem* 2017;**18**:1338−45.
28. Trott O, Olson AJ. AutoDock Vina: improving the speed and accuracy of docking with a new scoring function, efficient optimization, and multithreading. *J Comput Chem* 2010;**31**:455−61.
29. Aspinall R, Pitts D, Lapenna A, Mitchell W. Immunity in the elderly: the role of the thymus. *J Comp Pathol* 2010;**142**:S111−5.
30. Krysko DV, Garg AD, Kaczmarek A, Krysko O, Agostinis P, Vandenabeele P. Immunogenic cell death and DAMPs in cancer therapy. *Nat Rev Cancer* 2012;**12**:860−75.
31. Xie Q, Ding J, Chen Y. Role of $CD8^+$ T lymphocyte cells: interplay with stromal cells in tumor microenvironment. *Acta Pharm Sin B* 2021;**11**:1365−78.
32. Peng JR, Xiao Y, Yang Q, Liu QY, Chen Y, Shi K, et al. Intracellular aggregation of peptide-reprogrammed small molecule nanoassemblies enhances cancer chemotherapy and combinatorial immunotherapy. *Acta Pharm Sin B* 2021;**11**:1069−82.
33. Dorshkind K, Rodriguez EM, Raj Signer. The ageing immune system: is it ever too old to become young again?. *Nat Rev Immunol* 2009;**9**:57−62.
34. Mancuso S, Carlisi M, Santoro M, Napolitano M, Raso S, Siragusa S. Immunosenescence and lymphomagenesis. *Immun Ageing* 2018;**15**:22.
35. Jones D, Wang ZX, Chen LX, Zhang S, Banerji R, Lei PJ, et al. Solid stress impairs lymphocyte infiltration into lymph-node metastases. *Nat Biomed Eng* 2021;**5**:1426−36.
36. Bois HD, Heim TA, Lund AW. Tumor-draining lymph nodes: at the crossroads of metastasis and immunity. *Sci Immunol* 2021;**6**:eabg3551.
37. Oo Okwudiri, Lore D, Rose N, Nuvagah FL, Ivan B, Marc DW, et al. Chemotherapy-induced changes and immunosenescence of $CD8^+$ T-cells in patients with breast cancer. *Anticancer Res* 2015;**35**:1481−9.
38. Kroemer G, Galluzzi L, Kepp O, Zitvogel L. Immunogenic cell death in cancer therapy. *Annu Rev Immunol* 2013;**31**:51−72.
39. Zhai WJ, Zhou XM, Wang HF, Li WQ, Chen GY, Sui XH, et al. A novel cyclic peptide targeting LAG-3 for cancer immunotherapy by activating antigen-specific $CD8^+$ T cell responses. *Acta Pharm Sin B* 2020;**10**:1047−60.
40. Zhao QF, Yang Y, Wang HL, Lei W, Liu YX, Wang SL. Gold nanoparticles modified hollow carbon system for dual-responsive release and chemo-photothermal synergistic therapy of tumor. *J Colloid Interface Sci* 2019;**554**:239−49.

41. Li X, Luo LH, Jiang MS, Zhu CQ, Shi YY, Zhang JL, et al. Cocktail strategy for 'cold' tumors therapy *via* active recruitment of $CD8^+$ T cells and enhancing their function. *J Contr Release* 2021;**334**: 413−26.
42. Li W, Yang J, Luo LH, Jiang MS, Qin B, Yin H, et al. Targeting photodynamic and photothermal therapy to the endoplasmic reticulum enhances immunogenic cancer cell death. *Nat Commun* 2019;**10**:3349.
43. Liu P, Xie X, Liu M, Hu S, Ding JS, Zhou WH. A smart MnO_2-doped graphene oxide nanosheet for enhanced chemo-photodynamic combinatorial therapy *via* simultaneous oxygenation and glutathione depletion. *Acta Pharm Sin B* 2021;**11**:823−34.